

Selected Topics in Computational Quantum Physics

量子物理计算方法选讲

Shuo Yang (杨硕)

Department of Physics, Tsinghua University

Email: shuoyang@tsinghua.edu.cn

WeChat: condmat-ys

Exact Diagonalization (ED)

$$H|\Psi\rangle = E|\Psi\rangle$$

- main idea
- matrix representation of Hamiltonian
- implement symmetries
- Lanczos method
- time evolution
- finite temperature
- various applications

Iterative diagonalization

- if only the ground state and the low-lying excited states are required, powerful iterative diagonalization procedures exist
- matrix dimension can be four or five orders of magnitude larger than complete diagonalization
- can be extended to investigate dynamical properties, time evolution, and the finite-temperature behaviors of the system
- example: Lanczos method, Jacobi-Davidson algorithm, restarted Arnoldi method
- open source packages (e.g., ARPACK) are available and widely used

scipy.sparse.linalg.eigs

```
scipy.sparse.linalg.eigs(A, k=6, M=None, sigma=None, which='LM', v0=None, ncv=None,  
maxiter=None, tol=0, return_eigenvectors=True, Minv=None, OPinv=None, OOppart=None)
```

Find k eigenvalues and eigenvectors of the square matrix A.

[[source](#)]

Variational principle

- we can find the ground state $|\Psi_0\rangle$ and its energy E_0 for a Hamiltonian H from the variational principle

the **wave-function functional** $E[\Psi] = \frac{\langle \Psi | H | \Psi \rangle}{\langle \Psi | \Psi \rangle}$ is minimized for $\Psi = \Psi_0$

with $E[\Psi_0] = E_0$

- the functional gradient gives the direction of steepest ascent of the functional from the point $|\Psi\rangle$

$$\frac{\partial E[\Psi]}{\partial \langle \Psi |} = \frac{H |\Psi\rangle}{\langle \Psi | \Psi \rangle} - \frac{\langle \Psi | H | \Psi \rangle |\Psi\rangle}{\langle \Psi | \Psi \rangle^2} = \frac{H |\Psi\rangle - E[\Psi] |\Psi\rangle}{\langle \Psi | \Psi \rangle} = |\Psi_a\rangle$$

- moving in the opposite direction will result in a wave function with lower energy for small positive α

$$E[\Psi - \alpha \Psi_a] < E[\Psi]$$

- to find the optimum value of α , it is convenient to introduce an **orthogonal basis** in the space spanned by two vectors

$$\{ |\Psi\rangle, |\Psi_a\rangle \} = \{ |\Psi\rangle, H |\Psi\rangle \}$$

Variational principle

- as the **first vector**, we normalize

$$|v_0\rangle = |\Psi\rangle / \sqrt{\langle\Psi|\Psi\rangle}$$

- for the **second vector** we orthogonalize $H|v_0\rangle$ to $|v_0\rangle$

$$|\tilde{v}_1\rangle = H|v_0\rangle - |v_0\rangle\langle v_0|H|v_0\rangle$$

and normalize to obtain $|v_1\rangle$, namely $|\tilde{v}_1\rangle = b_0|v_1\rangle$, $\langle v_1|v_1\rangle = 1$, $\langle\tilde{v}_1|\tilde{v}_1\rangle = b_0^2$

- with $a_n = \langle v_n|H|v_n\rangle$, we have

$$H|v_0\rangle = |\tilde{v}_1\rangle + |v_0\rangle\langle v_0|H|v_0\rangle = b_0|v_1\rangle + a_0|v_0\rangle$$

we see that

$$\langle v_1|H|v_0\rangle = b_0$$

- in the basis $\{|v_0\rangle, |v_1\rangle\}$, the **Hamiltonian matrix** is given by

$$H_{\{|\Psi\rangle, H|\Psi\rangle\}} = \begin{pmatrix} a_0 & b_0 \\ b_0 & a_1 \end{pmatrix}$$

- we find a lower energy state $|\Psi'\rangle$ by diagonalizing the above Hamiltonian
- starting from $|\Psi'\rangle$, we may repeat the above steps to find the ground state

Power method

- the eigenstate with the extremal eigenvalue is obtained by repeatedly applying the Hamiltonian to a random initial state $|v_0\rangle$

$$|v_n\rangle = H^n |v_0\rangle$$

expanding in the eigenbasis

$$|v_n\rangle = H^n \left[\sum_i |i\rangle\langle i| \right] |v_0\rangle = \sum_i \langle i| v_0 \rangle H^n |i\rangle = \sum_i \langle i| v_0 \rangle \lambda_i^n |i\rangle$$

- the state with the eigenvalue with the largest absolute value will have the highest weight after many iterations n , provided that $|v_0\rangle$ has a finite overlap with this state
- the convergence of the power method is generally much poorer than other methods, it is generally not used in practice
- very simple to implement
memory efficient, only two vectors must be stored in memory

Krylov space

- a more efficient way is to consider not only $\{ |v_0\rangle, H|v_0\rangle \}$ or only $H^n |v_0\rangle$ but the whole subspace of the Hilbert space spanned by the set of states
- the subspace generated by the sequence of steps in the power method

$$\left\{ |v_0\rangle, H|v_0\rangle, H^2|v_0\rangle, \dots, H^n|v_0\rangle \right\}$$

is called the n^{th} Krylov space

- in this subspace, an optimal linear combination of vectors approximating the extremal eigenstate exists, and the way to find it is to diagonalize H in the generated subspace of $n + 1$ vectors
- can also accurately reproduce a number of low-lying excited states
- apply to eigenvalue problems more generally as well
widely used in many areas of science and engineering

Lanczos method

Lanczos, C. "An iteration method for the solution of the eigenvalue problem of linear differential and integral operators", J. Res. Nat'l Bur. Std. 45, 255-282 (1950).



- start from an arbitrary normalized state $|\phi_0\rangle$
only requirement of $|\phi_0\rangle$: it is not orthogonal to the ground state of H
randomly generated, or something known to have a large overlap
- our aim: write H in as a tridiagonal matrix

$$H = \begin{pmatrix} a_0 & b_0 & 0 & \cdots & 0 \\ b_0 & a_1 & b_1 & \ddots & \vdots \\ 0 & b_1 & a_2 & \ddots & 0 \\ \vdots & \ddots & \ddots & \ddots & b_{n-1} \\ 0 & \cdots & 0 & b_{n-1} & a_n \end{pmatrix}$$

on a set of basis $\{|\phi_0\rangle, |\phi_1\rangle, \dots, |\phi_n\rangle\}$

Lanczos method

- the iterative procedure to construct Lanczos basis $\{|\phi_0\rangle, |\phi_1\rangle, \dots, |\phi_n\rangle\}$ is

$$|\phi_1\rangle = \frac{1}{b_0}(H|\phi_0\rangle - a_0|\phi_0\rangle), \quad a_0 = \langle\phi_0|H|\phi_0\rangle$$

$$|\phi_2\rangle = \frac{1}{b_1}(H|\phi_1\rangle - a_1|\phi_1\rangle - b_0|\phi_0\rangle), \quad a_1 = \langle\phi_1|H|\phi_1\rangle$$

$$|\phi_3\rangle = \frac{1}{b_2}(H|\phi_2\rangle - a_2|\phi_2\rangle - b_1|\phi_1\rangle), \quad a_2 = \langle\phi_2|H|\phi_2\rangle$$

...

...

- in general

$$|\phi_{m+1}\rangle = \frac{1}{b_m}(H|\phi_m\rangle - a_m|\phi_m\rangle - b_{m-1}|\phi_{m-1}\rangle), \quad a_m = \langle\phi_m|H|\phi_m\rangle$$

where b_m is a real number to ensure $\langle\phi_{m+1}|\phi_{m+1}\rangle = 1$, and $|\phi_{-1}\rangle = 0$, $b_{-1} = 0$

- we show $\{|\phi_0\rangle, |\phi_1\rangle, \dots, |\phi_n\rangle\}$ is a set of orthogonal basis in three steps

$$\langle\phi_m|\phi_{m+1}\rangle = 0,$$

$$\langle\phi_{m-1}|\phi_{m+1}\rangle = 0,$$

$$\langle\phi_{m-k}|\phi_{m+1}\rangle = 0, \quad k > 1$$

Orthogonal basis

- we notice that $\langle \phi_0 | \phi_1 \rangle = \frac{1}{b_1} (\langle \phi_0 | H | \phi_0 \rangle - a_0 \langle \phi_0 | \phi_0 \rangle) = 0$

suppose $\langle \phi_{m-1} | \phi_m \rangle = 0$, we show that

$$\boxed{\langle \phi_m | \phi_{m+1} \rangle = \frac{1}{b_m} (\langle \phi_m | H | \phi_m \rangle - a_m \langle \phi_m | \phi_m \rangle - b_{m-1} \langle \phi_m | \phi_{m-1} \rangle)} = 0$$

- we notice that

$$\begin{aligned}\langle \phi_0 | \phi_2 \rangle &= \frac{1}{b_1} (\langle \phi_0 | H | \phi_1 \rangle - a_1 \langle \phi_0 | \phi_1 \rangle - b_0 \langle \phi_0 | \phi_0 \rangle) = \frac{1}{b_1} ([b_0 \langle \phi_1 | + a_0 \langle \phi_0 |] | \phi_1 \rangle - 0 - b_0) \\ &= \frac{1}{b_1} (b_0 \langle \phi_1 | \phi_1 \rangle + a_0 \langle \phi_0 | \phi_1 \rangle - 0 - b_0) = 0\end{aligned}$$

suppose $\langle \phi_{m-2} | \phi_m \rangle = 0$, we show that

$$\begin{aligned}\boxed{\langle \phi_{m-1} | \phi_{m+1} \rangle} &= \frac{1}{b_m} (\langle \phi_{m-1} | H | \phi_m \rangle - a_m \langle \phi_{m-1} | \phi_m \rangle - b_{m-1} \langle \phi_{m-1} | \phi_{m-1} \rangle) \\ &= \frac{1}{b_m} ([b_{m-1} \langle \phi_m | + a_{m-1} \langle \phi_{m-1} | + b_{m-2} \langle \phi_{m-2} |] | \phi_m \rangle - 0 - b_{m-1}) \\ &= \frac{1}{b_m} (b_{m-1} \langle \phi_m | \phi_m \rangle + a_{m-1} \langle \phi_{m-1} | \phi_m \rangle + b_{m-2} \langle \phi_{m-2} | \phi_m \rangle - 0 - b_{m-1}) \boxed{= 0}\end{aligned}$$

Orthogonal basis and matrix elements

- suppose $\langle \phi_{m-k} | \phi_{m-1} \rangle = 0, \langle \phi_{m-k} | \phi_m \rangle = 0, \langle \phi_{m-k+1} | \phi_m \rangle = 0, \langle \phi_{m-k-1} | \phi_m \rangle = 0,$

we show that for $k > 1$

$$\begin{aligned}\langle \phi_{m-k} | \phi_{m+1} \rangle &= \frac{1}{b_m} (\langle \phi_{m-k} | H | \phi_m \rangle - a_m \langle \phi_{m-k} | \phi_m \rangle - b_{m-1} \langle \phi_{m-k} | \phi_{m-1} \rangle) \\ &= \frac{1}{b_m} ([b_{m-k} \langle \phi_{m-k+1} | + a_{m-k} \langle \phi_{m-k} | + b_{m-k-1} \langle \phi_{m-k-1} |] | \phi_m \rangle - 0 - 0) = 0\end{aligned}$$

- therefore, $\{ |\phi_0\rangle, |\phi_1\rangle, \dots, |\phi_n\rangle \}$ is a set of orthogonal basis
- next, we show the matrix elements

$$\langle \phi_m | H | \phi_m \rangle = [b_m \langle \phi_{m+1} | + a_m \langle \phi_m | + b_{m-1} \langle \phi_{m-1} |] | \phi_m \rangle = a_m + 0 + 0 = a_m$$

$$\langle \phi_m | H | \phi_{m+1} \rangle = [b_m \langle \phi_{m+1} | + a_m \langle \phi_m | + b_{m-1} \langle \phi_{m-1} |] | \phi_{m+1} \rangle = b_m + 0 + 0 = b_m$$

$$\langle \phi_m | H | \phi_{m-1} \rangle = \langle \phi_m | [b_{m-1} \langle \phi_m | + a_{m-1} \langle \phi_{m-1} | + b_{m-2} \langle \phi_{m-2} |] = b_{m-1} + 0 + 0 = b_{m-1}$$

- when $k \geq 1$,

$$\langle \phi_{m-k} | H | \phi_{m+1} \rangle = [b_{m-k} \langle \phi_{m-k+1} | + a_{m-k} \langle \phi_{m-k} | + b_{m-k-1} \langle \phi_{m-k-1} |] | \phi_{m+1} \rangle = 0$$

Convergence of Lanczos calculations

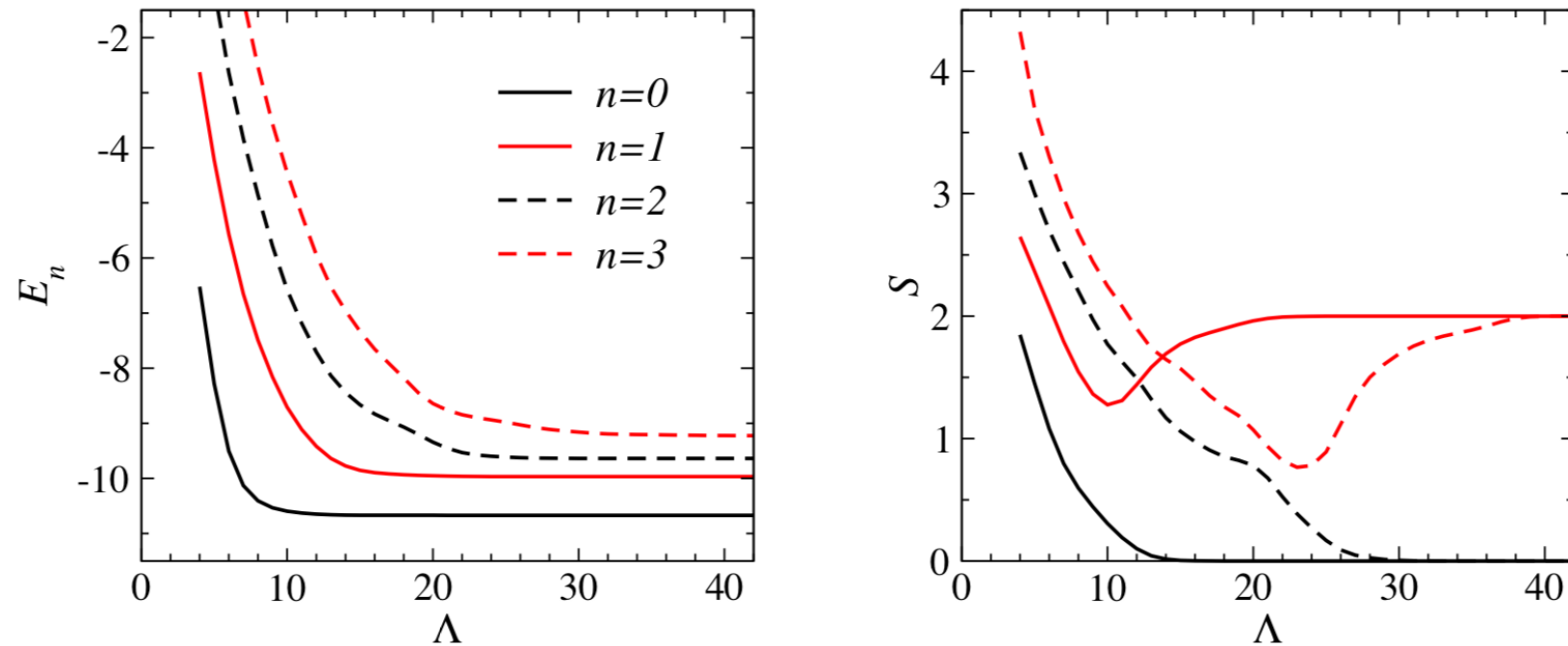


FIGURE 30. Example of the convergence as a function of the Lanczos basis size of the energy (left) and the total spin (right) of the four lowest levels of the 24-site Heisenberg chain in the symmetry sector $k = 0, p = 1, z = 1$. The spin S is extracted using the assumption that $\langle \mathbf{S}^2 \rangle = S(S + 1)$.

- number of Lanczos vectors needed: in the order of few tens to hundreds
- energies often converge faster than other observables

Convergence of Lanczos calculations

- drawback of Lanczos algorithms: loss of orthogonality

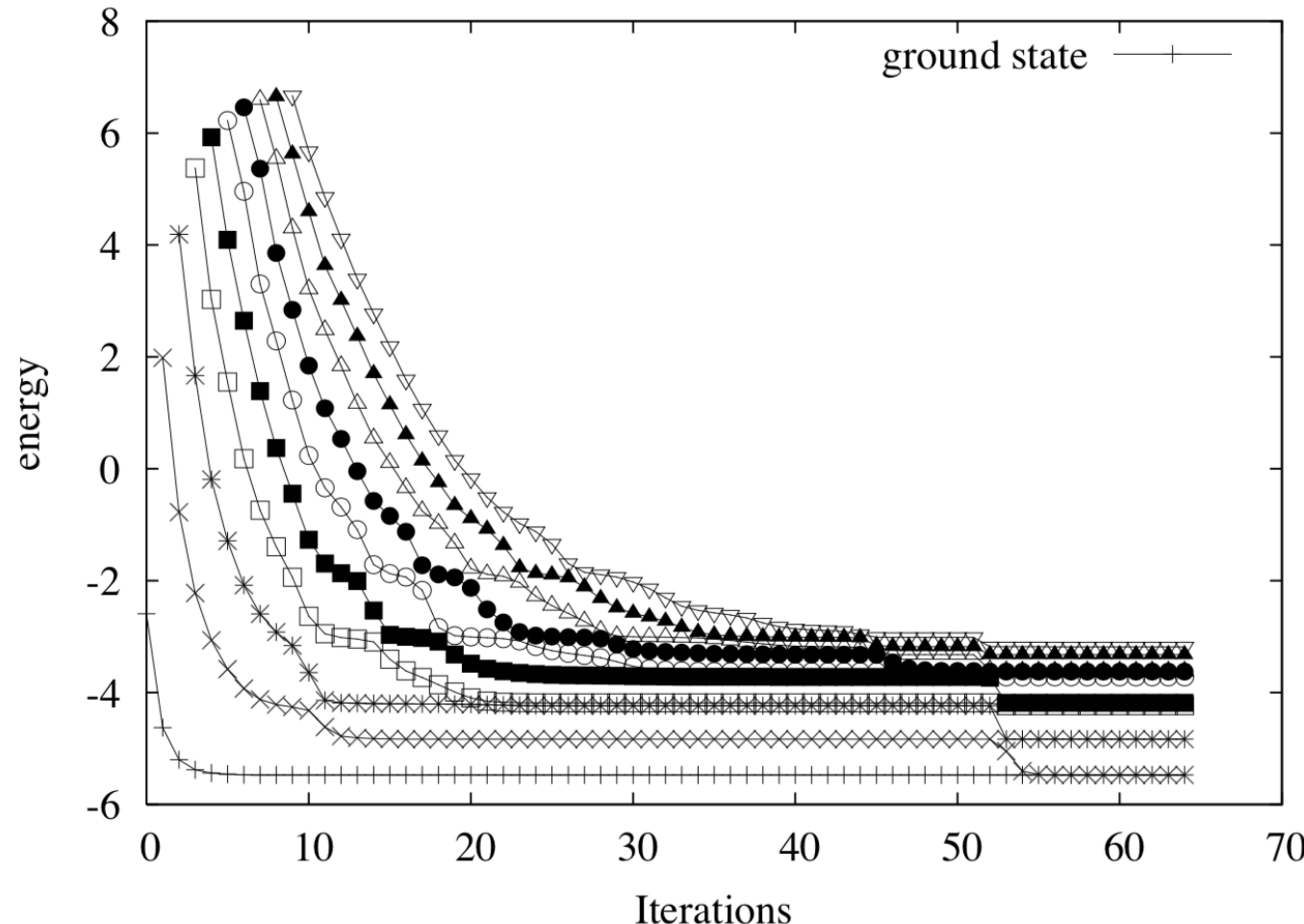


FIGURE 4. Typical convergence behavior of the Lanczos algorithm. In this example, convergence to the ground-state is already reached after approximately 10 iterations, while additional iterations are required to reach convergence for the excited states. “Ghost” eigenvalues appear and converge to a real eigenvalue as additional iterations are performed, leading to erroneous multiplicity at the completion of the calculation.

Reorthogonalize the Lanczos vectors

- straightforward solution, reorthogonalize Lanczos vectors relative to each other using a modified Gram-Schmidt procedure
- each new Lanczos vector constructed is explicitly orthogonalized with respect to all previous basis vectors

$$|\phi_{m+1}\rangle \rightarrow \frac{|\phi_{m+1}\rangle - q |\phi_i\rangle}{1 - q^2}, q = \langle \phi_i | \phi_{m+1} \rangle$$

- requires all vectors to be stored in memory, so that the advantage of memory efficiency is lost
- or start from the same initial state and re-calculate all vectors
- how to improve this?

Reorthogonalize the Lanczos vectors

- modified Lanczos method
 - only two Lanczos vectors are considered and the resulting 2×2 matrix is diagonalized
 - the resultant eigenvector is taken as the starting point for a new 2×2 Lanczos procedure
 - repeat until convergence
- only limited usage:
 - convergence is only marginally better than power method, difficult to obtain excited states
- implicitly Lanczos method
 - after 10 to 100 Lanczos iterations, the resulting tridiagonal matrix is diagonalized and the extremal eigenstate is used as starting vector for a new Lanczos procedure

Convergence of Lanczos calculations

- before and after orthogonality

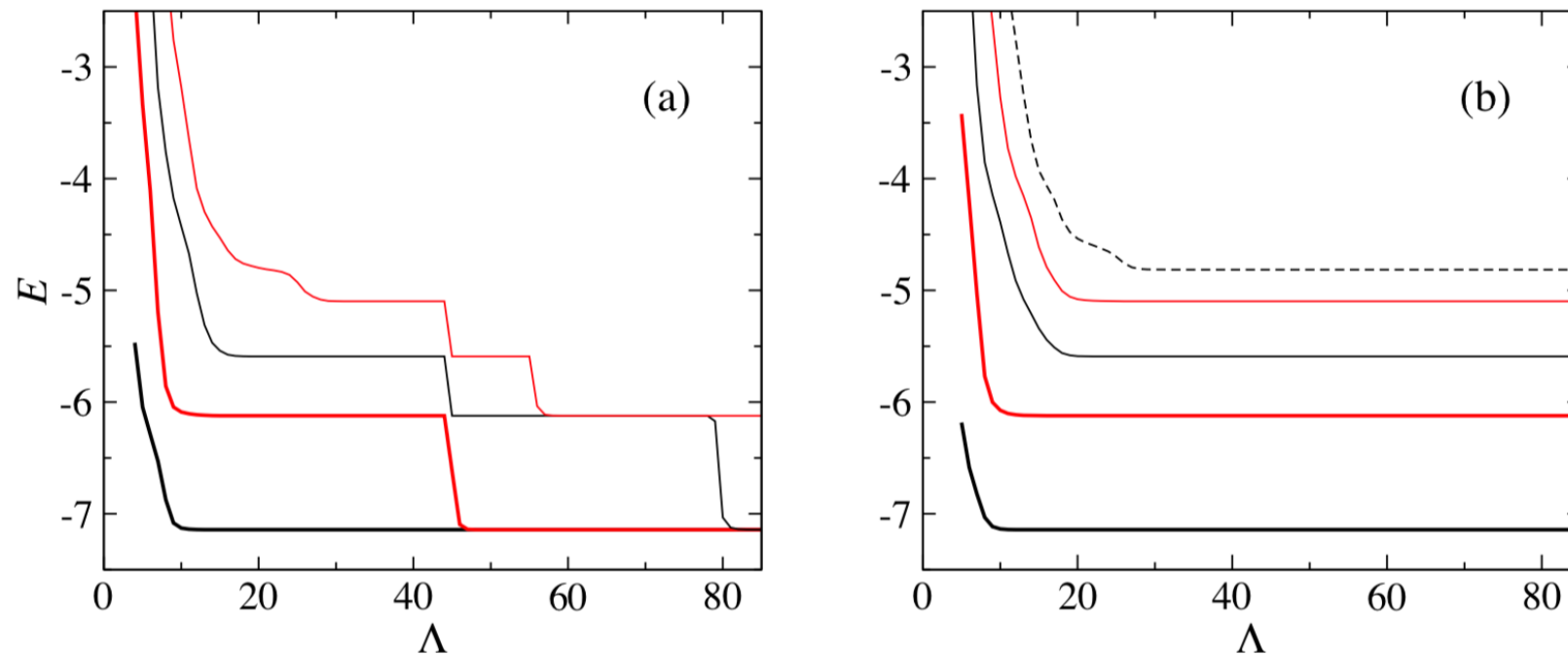


FIGURE 31. (a) The four lowest energies as a function of the Lanczos basis size for a 16-site Heisenberg chain with quantum numbers ($k = 0, p = 1, z = 1$). Multiple copies of the same state appear successively due to loss of orthogonality. (b) The five lowest states of the same system obtained with reorthogonalization of the basis set.

Classical Green's function

- imagine one would like to solve a partial linear inhomogeneous differential equation $Df(x) = g(x)$
- the particular solution $f(x)$ can be formally found with the aid of a function $G(x, x')$
$$f(x) = \int G(x, x')g(x')dx'$$
- the Green's function is defined as the solution of a differential equation

$$DG(x, x') = \delta(x - x')$$

- example: electric potential $\varphi(\mathbf{r})$ to a given charge density distribution $\rho(\mathbf{r})$

$$\nabla^2 \varphi(\mathbf{r}) = -\frac{\rho(\mathbf{r})}{\epsilon_0}$$

- the Green's function should satisfies $\boxed{\nabla^2 G(\mathbf{r}, \mathbf{r}') = \delta(\mathbf{r} - \mathbf{r}')}}$

we find the solution
$$G(\mathbf{r}, \mathbf{r}') = -\frac{1}{4\pi} \frac{1}{|\mathbf{r} - \mathbf{r}'|}$$

- for an arbitrary charge density distribution, the solution of $\varphi(\mathbf{r})$ is

$$\varphi(\mathbf{r}) = \frac{1}{4\pi\epsilon_0} \int \frac{\rho(\mathbf{r}')}{|\mathbf{r} - \mathbf{r}'|} d\mathbf{r}'$$

Quantum Green's function

- from the Schroedinger's equation

$$i\hbar \frac{\partial}{\partial t} \Psi(\mathbf{r}, t) = H\Psi(\mathbf{r}, t) = \left[-\frac{\hbar^2}{2m} \nabla^2 + V(\mathbf{r}, t) \right] \Psi(\mathbf{r}, t)$$

$$\left[i\hbar \frac{\partial}{\partial t} + \frac{\hbar^2}{2m} \nabla^2 \right] \Psi(\mathbf{r}, t) = V(\mathbf{r}, t) \Psi(\mathbf{r}, t)$$

- instead of solving Schroedinger's equation, we can equivalently look for the **Green's function** that solves

$$\left[i\hbar \frac{\partial}{\partial t} + \frac{\hbar^2}{2m} \nabla^2 \right] G(\mathbf{r}, t; \mathbf{r}', t') = \delta(\mathbf{r} - \mathbf{r}') \delta(t - t')$$

- after that, the solution of $\Psi(\mathbf{r}, t)$ may be written as

$$\Psi(\mathbf{r}, t) = \int G(\mathbf{r}, t; \mathbf{r}', t') V(\mathbf{r}', t') \Psi(\mathbf{r}', t') d^3 r'$$

- the equation above describes the time evolution of the wave function from (\mathbf{r}', t') to (\mathbf{r}, t)

Green's function is known as the **propagator**

$$G(\mathbf{r}, t; \mathbf{r}', t') = \langle \mathbf{r} | e^{-\frac{i}{\hbar} H(t-t')} | \mathbf{r}' \rangle = \langle \mathbf{r}, t | \mathbf{r}', t' \rangle$$

Green's function

- causal Green's function

$$\begin{aligned} G_{i,j}^c(t, t') &= -i\langle T[c_i(t)c_j^\dagger(t')]\rangle = -i\theta(t-t')\langle c_i(t)c_j^\dagger(t')\rangle + i\theta(t'-t)\langle c_j^\dagger(t')c_i(t)\rangle \\ &= \theta(t-t')G_{i,j}^>(t, t') + \theta(t'-t)G_{i,j}^<(t, t') \end{aligned}$$

where $\theta(x)$ is the Heaviside step function $\theta(x) = \begin{cases} 1, & \text{for } x > 0 \\ 0, & \text{for } x < 0 \end{cases}$

- retarded Green's function

$$G_{i,j}^r(t, t') = -i\theta(t-t')\langle \{c_i(t), c_j^\dagger(t')\}\rangle = \theta(t-t')(G_{i,j}^>(t, t') - G_{i,j}^<(t, t'))$$

- advanced Green's function

$$G_{i,j}^a(t, t') = i\theta(t'-t)\langle \{c_i(t), c_j^\dagger(t')\}\rangle = -\theta(t'-t)(G_{i,j}^>(t, t') - G_{i,j}^<(t, t'))$$

- lesser Green's function $G_{i,j}^<(t, t') = i\langle c_j^\dagger(t')c_i(t)\rangle$
- greater Green's function = correlation function $G_{i,j}^>(t, t') = -i\langle c_i(t)c_j^\dagger(t')\rangle$
- connection between Green's functions

$$G_{i,j}^r(t, t') - G_{i,j}^a(t, t') = G_{i,j}^>(t, t') - G_{i,j}^<(t, t')$$

Dynamical properties

- we are interested in calculating time-dependent correlation functions

$$C(t) = -i\langle \Phi_0 | A(t)A^\dagger(0) | \Phi_0 \rangle$$

where A generates the desired correlations, $|\Phi_0\rangle$ is the ground state

- for $t > 0$, we have

$$\begin{aligned} C(t) &= -i\theta(t)\langle \Phi_0 | e^{iHt}A(0)e^{-iHt}A^\dagger(0) | \Phi_0 \rangle \\ &= -i\left(-\frac{1}{2\pi i}\int_{-\infty}^{\infty} d\omega \frac{e^{-i\omega t}}{\omega + i\eta}\right)e^{iE_0 t}\langle \Phi_0 | A(0)e^{-iHt}A^\dagger(0) | \Phi_0 \rangle \\ &= \frac{1}{2\pi}\int_{-\infty}^{\infty} d\omega \langle \Phi_0 | A(0) \frac{e^{-i(\omega+H-E_0)t}}{\omega + i\eta} A^\dagger(0) | \Phi_0 \rangle \\ &= \frac{1}{2\pi}\int_{-\infty}^{\infty} d\omega \langle \Phi_0 | A(0) \frac{e^{-i\omega t}}{\omega + i\eta - H + E_0} A^\dagger(0) | \Phi_0 \rangle = \frac{1}{2\pi}\int_{-\infty}^{\infty} d\omega e^{-i\omega t} C(\omega + i\eta) \end{aligned}$$

- we obtain the Fourier transform of $C(t)$ to frequency space

$$C(\omega + i\eta) = \langle \Phi_0 | A(0) \frac{1}{\omega + i\eta - H + E_0} A^\dagger(0) | \Phi_0 \rangle$$

Local density of states

$$\begin{aligned}
C_{jj,\sigma}(\omega + i\eta) &= \langle \Phi_0 | C_{j,\sigma} \frac{1}{\omega + i\eta - H + E_0} C_{j,\sigma}^\dagger | \Phi_0 \rangle \\
&= \sum_{mn} \langle \Phi_0 | C_{j,\sigma} | \Phi_m \rangle \langle \Phi_m | \frac{1}{\omega + i\eta - H + E_0} | \Phi_n \rangle \langle \Phi_n | C_{j,\sigma}^\dagger | \Phi_0 \rangle \\
&= \sum_n |\langle \Phi_n | C_{j,\sigma}^\dagger | \Phi_0 \rangle|^2 \frac{1}{\omega - (E_n - E_0) + i\eta}
\end{aligned}$$

- using the identity

$$\lim_{\eta \rightarrow 0^+} \frac{1}{\omega - \epsilon \pm i\eta} = \mathcal{P}\left(\frac{1}{\omega - \epsilon}\right) \mp i\pi\delta(\omega - \epsilon)$$

we obtain $\lim_{\eta \rightarrow 0^+} \text{Im}C_{jj,\sigma}(\omega + i\eta) = (\lim_{\eta \rightarrow 0^+} C_{jj,\sigma}(\omega + i\eta) - \lim_{\eta \rightarrow 0^+} C_{jj,\sigma}^\dagger(\omega + i\eta))/(2i)$

$$= -\pi \sum_n |\langle \Phi_n | C_{j,\sigma}^\dagger | \Phi_0 \rangle|^2 \delta[\omega - (E_n - E_0)]$$

- the local density of states of a discrete spectrum is

$$\rho_{j,\sigma}(\omega) = \sum_n |\langle \Phi_n | C_{j,\sigma}^\dagger | \Phi_0 \rangle|^2 \delta[\omega - (E_n - E_0)]$$

- the imaginary part of $C_{jj,\sigma}(\omega + i\eta)$ provides the local density of states

$$\rho_{j,\sigma}(\omega) = -\frac{1}{\pi} \lim_{\eta \rightarrow 0^+} \text{Im}C_{jj,\sigma}(\omega + i\eta)$$

Spectral function

- local density of states

$$\rho_{j,\sigma}(\omega) = -\frac{1}{\pi} \lim_{\eta \rightarrow 0^+} \text{Im} C_{jj,\sigma}(\omega + i\eta) = -\frac{1}{\pi} \lim_{\eta \rightarrow 0^+} \text{Im} \langle \Phi_0 | C_{j,\sigma} \frac{1}{\omega + i\eta - H + E_0} C_{j,\sigma}^\dagger | \Phi_0 \rangle$$

- density of states $\rho(\omega) = \sum_{j,\sigma} \rho_{j,\sigma}(\omega)$

- in general, the **spectral function** is given by

$$I(\omega) = -\frac{1}{\pi} \lim_{\eta \rightarrow 0^+} \text{Im} C(\omega + i\eta) = -\frac{1}{\pi} \lim_{\eta \rightarrow 0^+} \{ \text{Im} [\langle \Phi_0 | A \frac{1}{\omega + i\eta - H + E_0} A^\dagger | \Phi_0 \rangle] \}$$

- spectral function can be probed in scattering experiments such as photoemission or neutron scattering

name	notation	operators	experiment
single-particle spectral weight	$A(\mathbf{k}, \omega)$	$A = c_{\mathbf{k},\sigma}$	photoemission
structure factor	$S_{zz}(\mathbf{q}, \omega)$	$A = S_{\mathbf{q}}^z$	neutron scattering
optical conductivity	$\sigma_{xx}(\omega)$	$A = j_x$	optics
4-spin correlation	$R(\omega)$	$A = \sum_{\mathbf{k}} R_{\mathbf{k}} \mathbf{S}_{\mathbf{k}} \cdot \mathbf{S}_{-\mathbf{k}}$	Raman scattering

Spectral function using Lanczos

- we are interested in calculating quantities such as

$$I(\omega) = -\frac{1}{\pi} \lim_{\eta \rightarrow 0^+} \{\text{Im}[\langle \Phi_0 | A^\dagger \frac{1}{\omega + i\eta - H + E_0} A | \Phi_0 \rangle]\} = -\frac{1}{\pi} \lim_{\eta \rightarrow 0^+} \{\text{Im}[\langle \Psi_0 | \frac{1}{z - H} | \Psi_0 \rangle]\}$$

where $|\Psi_0\rangle = A|\Phi_0\rangle$, and $z = \omega + i\eta + E_0$

we normalize $|\Psi_0\rangle$ into $|\phi_0\rangle = |\Psi_0\rangle/\alpha$, where $\langle \Psi_0 | \Psi_0 \rangle = \alpha^2$

- we restart from $|\phi_0\rangle$ to construct a new Krylov space

$z - H$ can be written in a tridiagonal form

$$z - H = \begin{pmatrix} z - a_0 & -b_0 & 0 & \cdots & 0 \\ -b_0 & z - a_1 & -b_1 & \ddots & \vdots \\ 0 & -b_1 & z - a_2 & \ddots & 0 \\ \vdots & \ddots & \ddots & \ddots & -b_{n-1} \\ 0 & \cdots & 0 & -b_{n-1} & z - a_n \end{pmatrix}$$

- the (0,0) element of the inverse of the above matrix gives $\langle \phi_0 | \frac{1}{z - H} | \phi_0 \rangle$

Spectral function using Lanczos

- the inverse of a block matrix is given by

$$\begin{pmatrix} A & B \\ C & D \end{pmatrix}^{-1} = \begin{pmatrix} (A - BD^{-1}C)^{-1} & -(A - BD^{-1}C)^{-1}BD^{-1} \\ -D^{-1}C(A - BD^{-1}C)^{-1} & D^{-1} + D^{-1}C(A - BD^{-1}C)^{-1}BD^{-1} \end{pmatrix}$$

- $z - H$ satisfies the following relation

$$z - H = \left(\begin{array}{c|ccccc} z - a_0 & -b_0 & 0 & \cdots & 0 \\ \hline -b_0 & z - a_1 & -b_1 & \ddots & \vdots \\ 0 & -b_1 & z - a_2 & \ddots & 0 \\ \vdots & \ddots & \ddots & \ddots & -b_{n-1} \\ 0 & \cdots & 0 & -b_{n-1} & z - a_n \end{array} \right) = \begin{pmatrix} z - a_0 & B \\ C & z - H_1 \end{pmatrix}$$

- we can show that

$$\begin{aligned} [(z - H)^{-1}]_{00} &= \frac{1}{z - a_0 - b_0^2[(z - H_1)^{-1}]_{00}} = \frac{1}{z - a_0 - \frac{b_0^2}{z - a_1 - b_1^2[(z - H_2)^{-1}]_{00}}} \\ &= \frac{1}{z - a_0 - \frac{b_0^2}{z - a_1 - \frac{b_1^2}{z - a_2 - \frac{b_2^2}{\dots}}}} \end{aligned}$$

Density of states

- 1D Hubbard chain

$$H = -t \sum_{j,\sigma} (C_{j,\sigma}^\dagger C_{j+1,\sigma} + C_{j+1,\sigma}^\dagger C_{j,\sigma}) + U \sum_j n_{j,\uparrow} n_{j,\downarrow} - \mu \sum_j (n_{j,\uparrow} + n_{j,\downarrow})$$

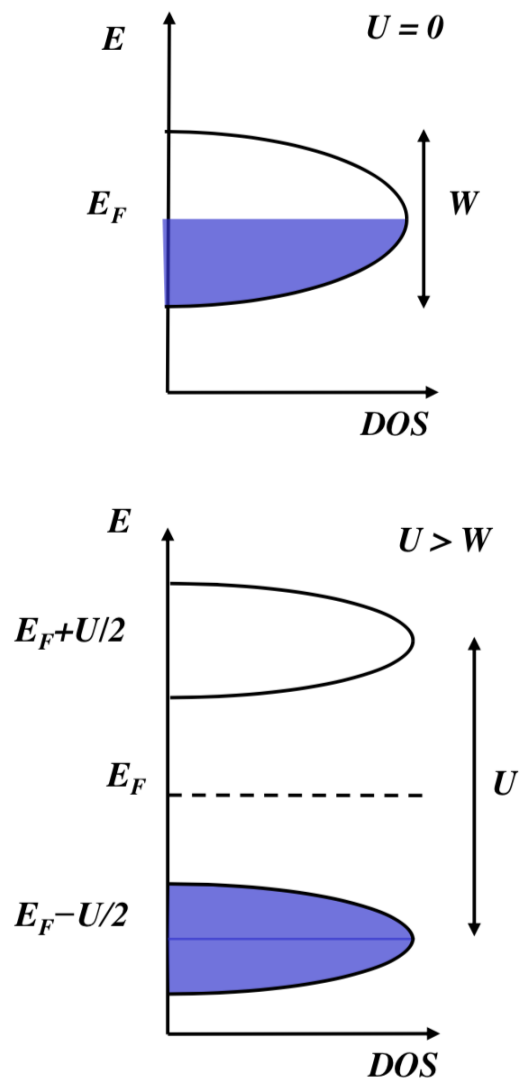
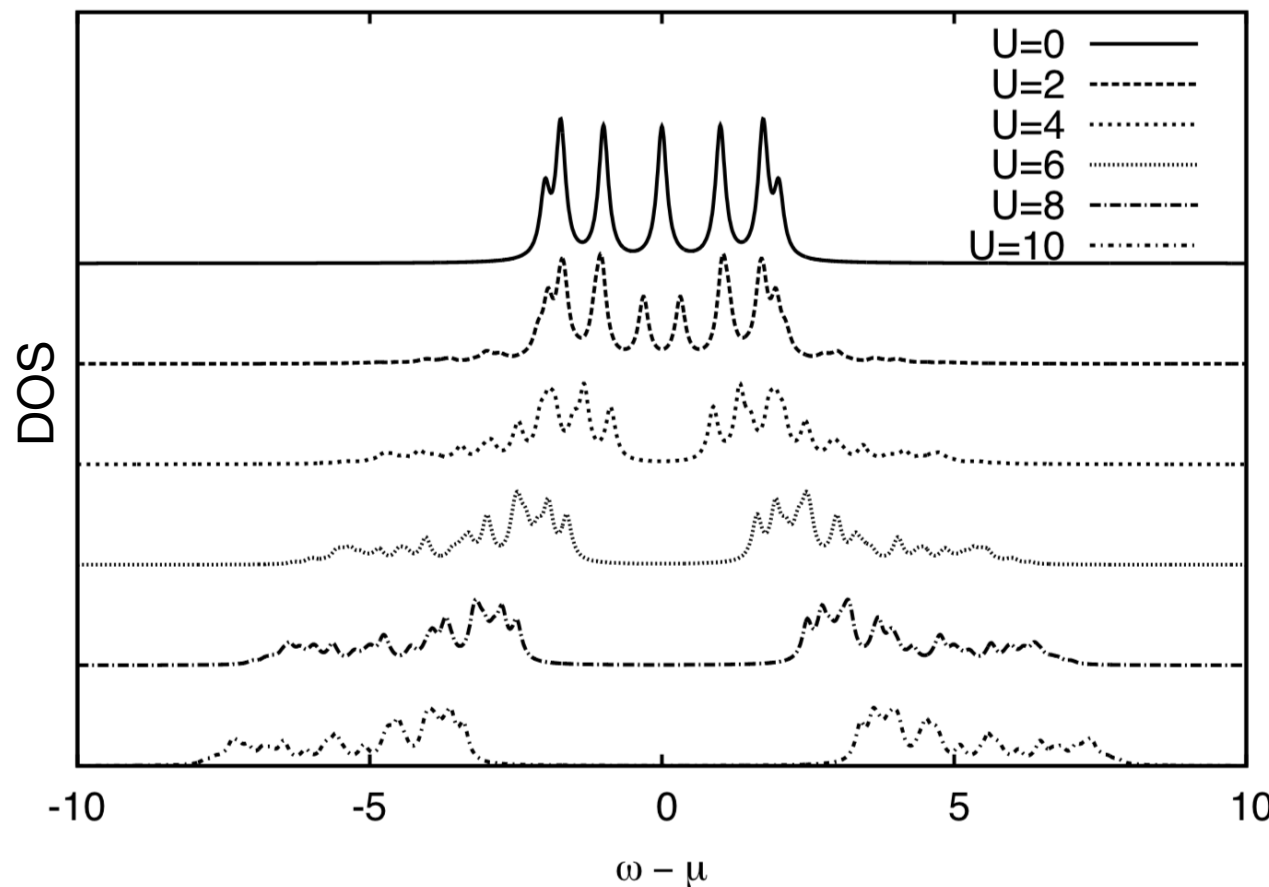


Figure 2.9: Mott insulator in one dimension for a 12 sites half-filled Hubbard chain (U as in image) with $t = 1$.

Density of states

- increasing the dimension of the Krylov space from 5 to 100

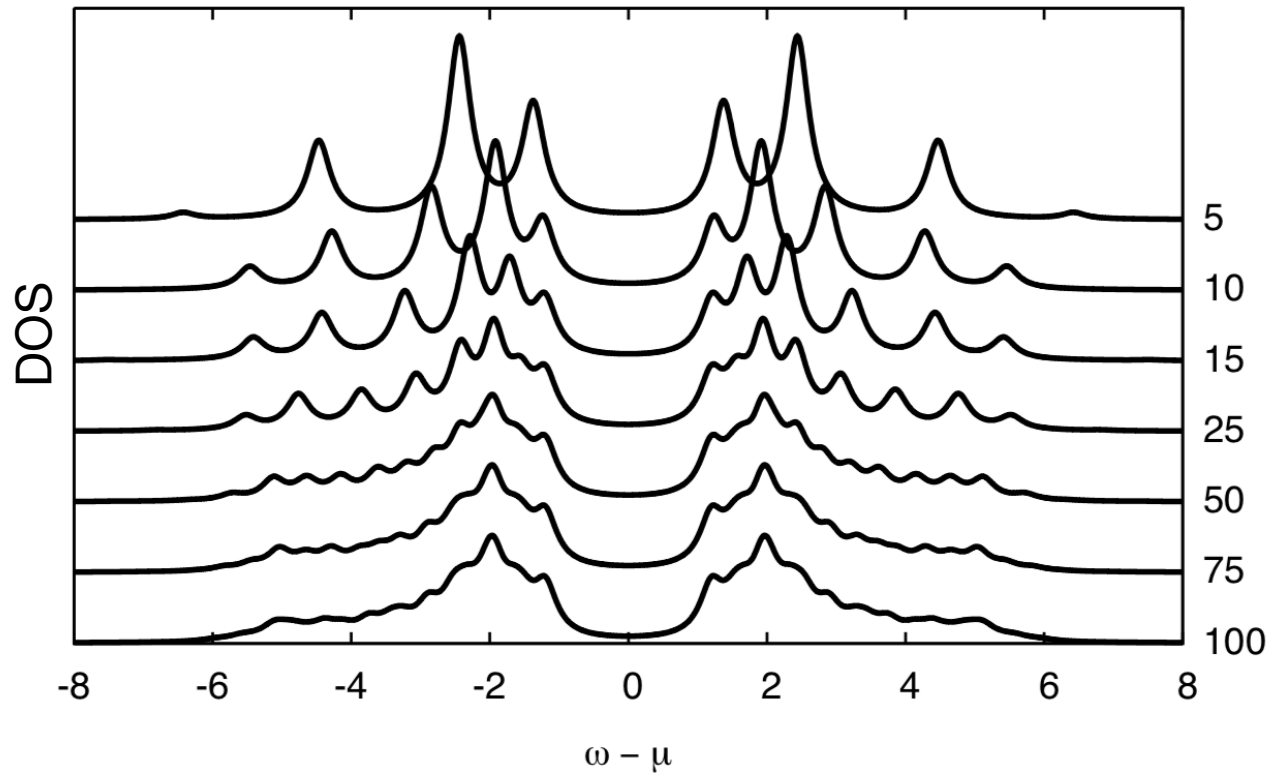
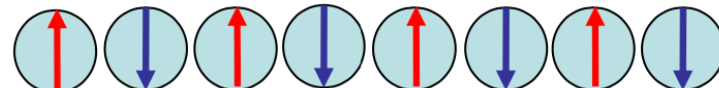


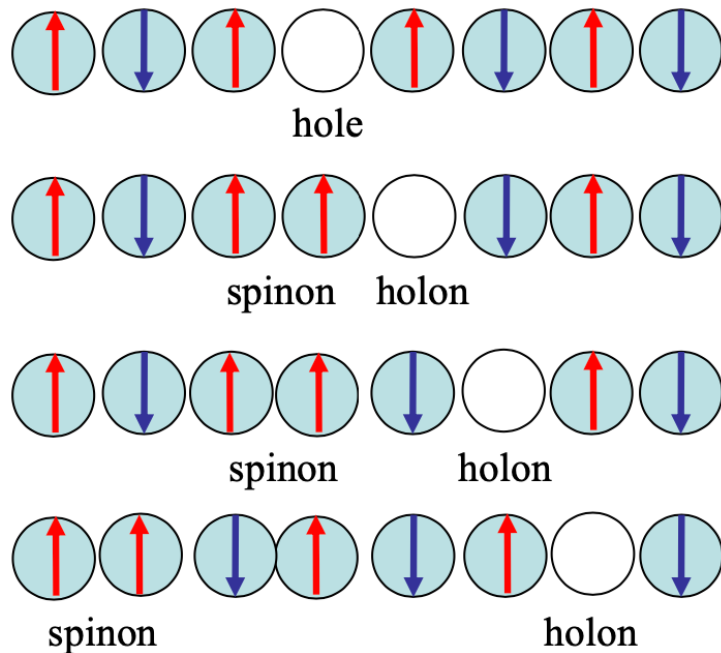
Fig. 4: Convergence of the spectral function with increasing number of Lanczos steps, $L=5, 10, 15, 25, 50, 75$, and 100 , for a 14-site Hubbard chain with $U = 5t$ at half filling. With increasing L , more and more moments of the photoemission and inverse photoemission part of the spectrum are reproduced correctly.

Spin-charge separation

$$H = -t \sum_{j,\sigma} (C_{j,\sigma}^\dagger C_{j+1,\sigma} + C_{j+1,\sigma}^\dagger C_{j,\sigma}) + U \sum_j n_{j,\uparrow} n_{j,\downarrow} - \mu \sum_j (n_{j,\uparrow} + n_{j,\downarrow})$$



- 1D chain with one electron per site with strong onsite Coulomb repulsion
the ground state is a Mott insulator with long-range AF ordering



- now take out an electron, like adding a hole
- the hole will propagate along the chain
it creates a spin excitation called “spinon”
and a vacancy of charge called “holon”
- the spinon and holon can propagate with different velocity
the spin and charge information are carried separately and independently

Spectral function $A(k, \omega)$

- TTF-TCNQ, quasi-1D conductor
1D Hubbard model, spin-charge separation

$$A(k, \omega) = \frac{1}{\pi} \text{Im} \langle \Phi_0 | C_{k,\sigma}^\dagger \frac{1}{\omega - i\eta + H - E_0} C_{k,\sigma} | \Phi_0 \rangle$$

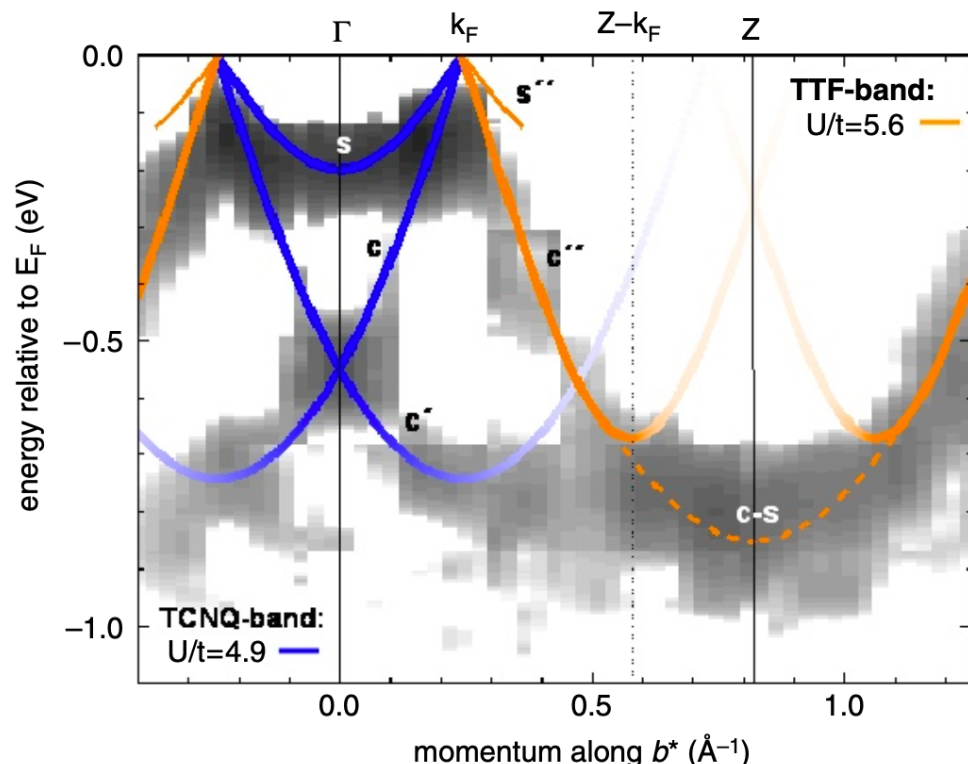
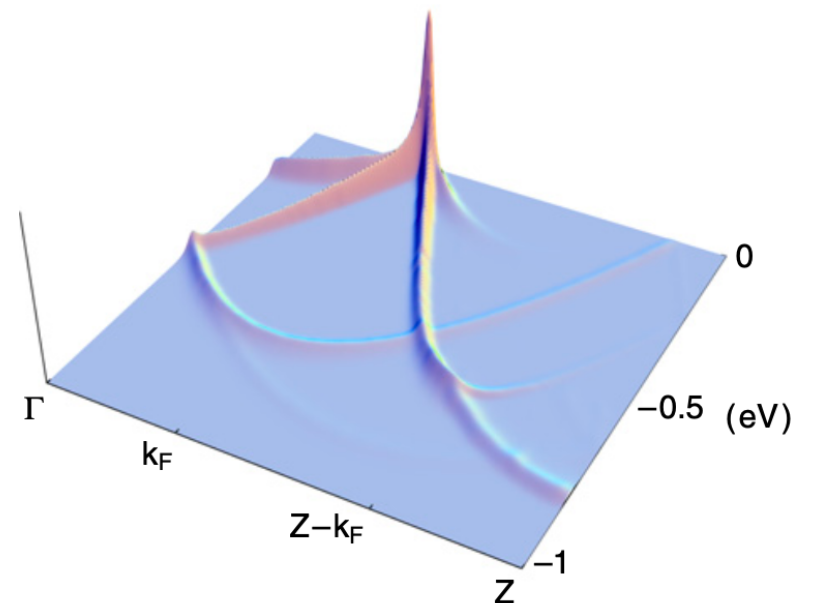
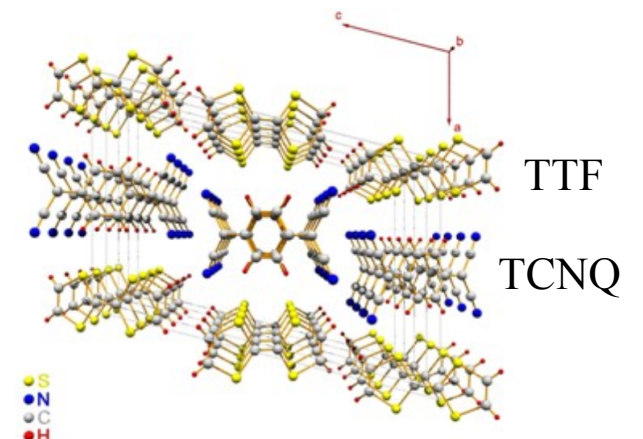
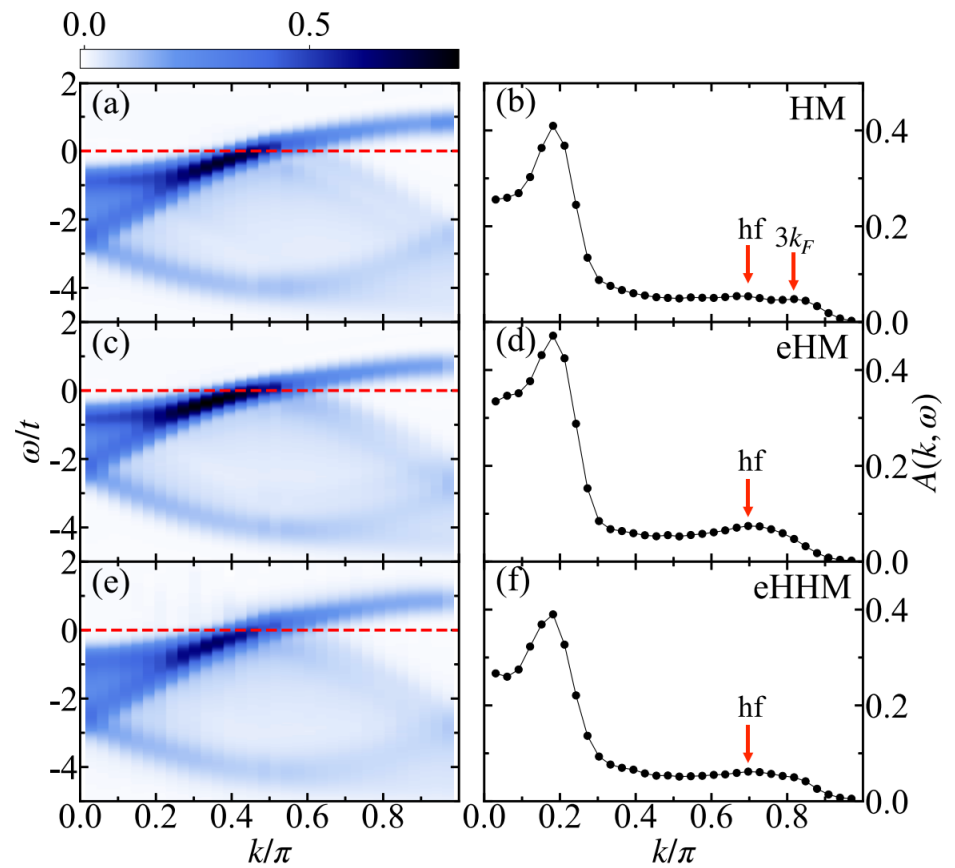
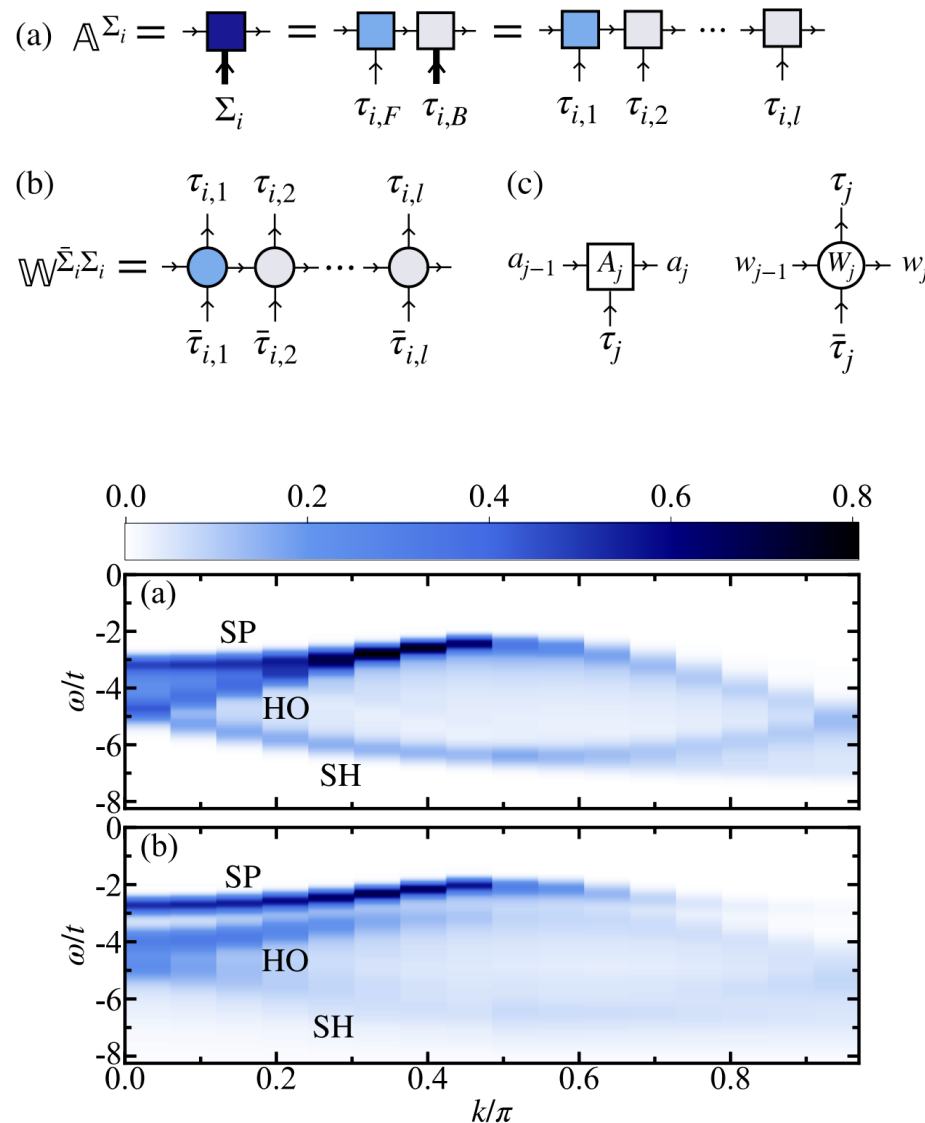


Figure 1. Experimental peak dispersions (gray scale) obtained by ARPES on TTF-TCNQ along the easy-transport axis as given in figure 7 of [4] and matching theoretical branch and border lines.

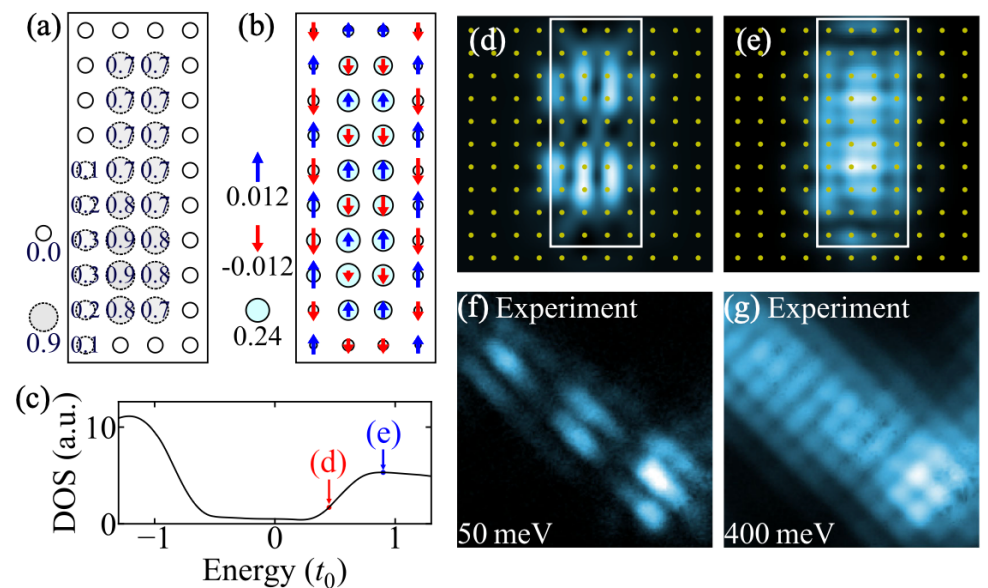
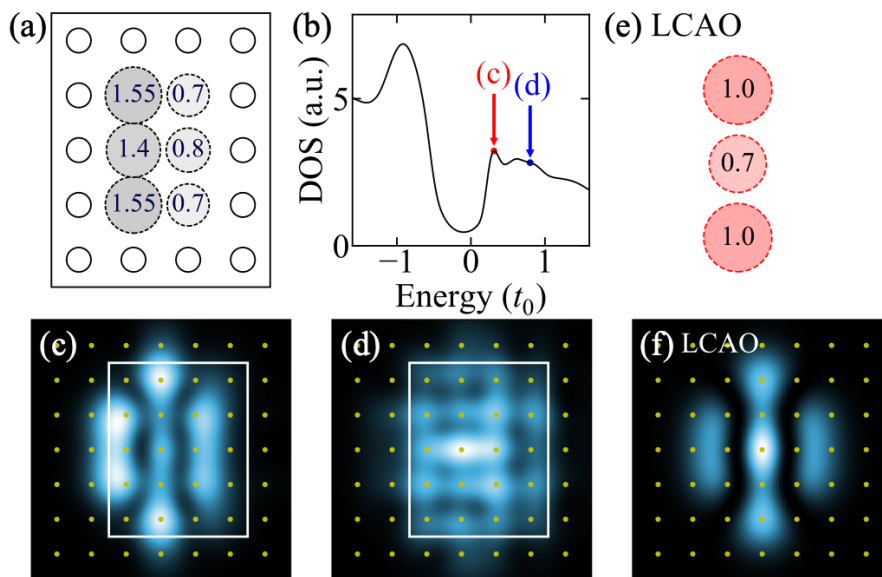
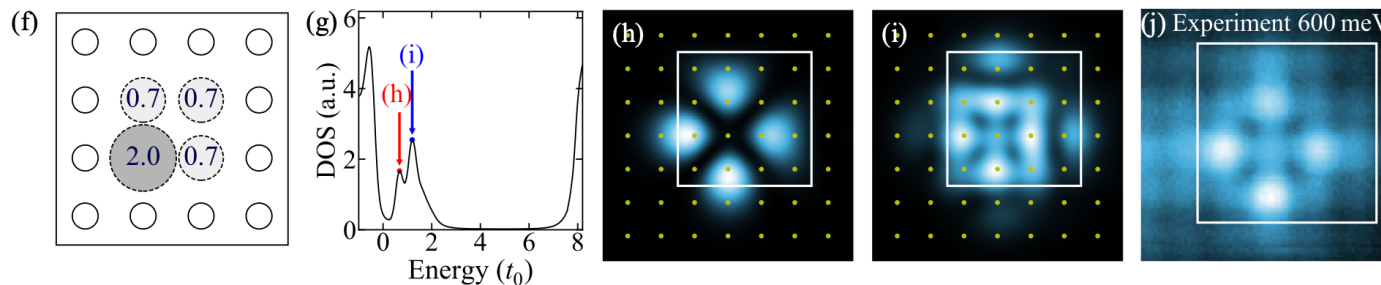
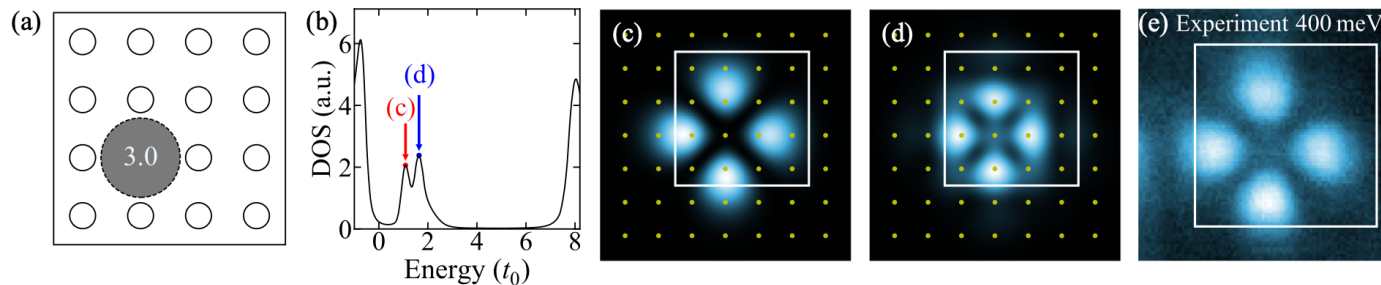


H. Benthien *et al*, PRL 92, 256401 (2004)
D. Bozi *et al*, J. Phys.: Condens. Matter 20, 022205 (2008)

Chebyshev pseudosite matrix product state approach for the spectral functions of electron-phonon coupling systems



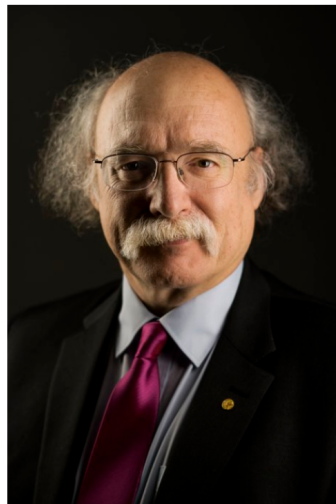
Unveiling Stripe-Shaped Charge Density Modulations in Doped Mott Insulators



Nobel prize in physics 2016



© Nobel Media AB. Photo: A.
Mahmoud
David J. Thouless
Prize share: 1/2



© Nobel Media AB. Photo: A.
Mahmoud
**F. Duncan M.
Haldane**
Prize share: 1/4



© Nobel Media AB. Photo: A.
Mahmoud
J. Michael Kosterlitz
Prize share: 1/4

- for theoretical discoveries of topological phase transitions and topological phases of matter

This year's Laureates opened the door on an unknown world where matter can assume strange states. They have used advanced mathematical methods to study unusual phases, or states, of matter, such as superconductors, superfluids or thin magnetic films. Thanks to their pioneering work, the hunt is now on for new and exotic phases of matter. Many people are hopeful of future applications in both materials science and electronics.

Quantum Hall effect without Landau levels

VOLUME 61, NUMBER 18

PHYSICAL REVIEW LETTERS

31 OCTOBER 1988

Model for a Quantum Hall Effect without Landau Levels: Condensed-Matter Realization of the “Parity Anomaly”

F. D. M. Haldane

Department of Physics, University of California, San Diego, La Jolla, California 92093

(Received 16 September 1987)

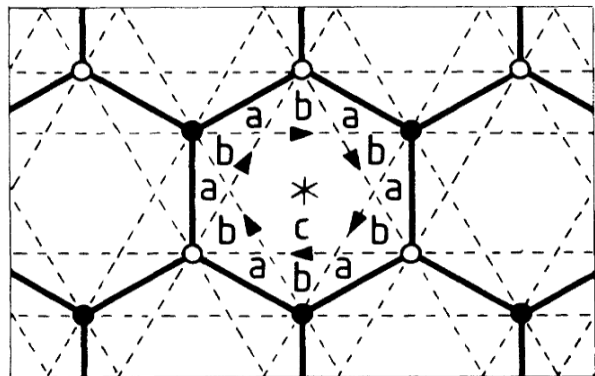


FIG. 1. The honeycomb-net model (“2D graphite”) showing nearest-neighbor bonds (solid lines) and second-neighbor bonds (dashed lines). Open and solid points, respectively, mark the *A* and *B* sublattice sites. The Wigner-Seitz unit cell is conveniently centered on the point of sixfold rotation symmetry (marked “*”) and is then bounded by the hexagon of nearest-neighbor bonds. Arrows on second-neighbor bonds mark the directions of positive phase hopping in the state with broken time-reversal invariance.

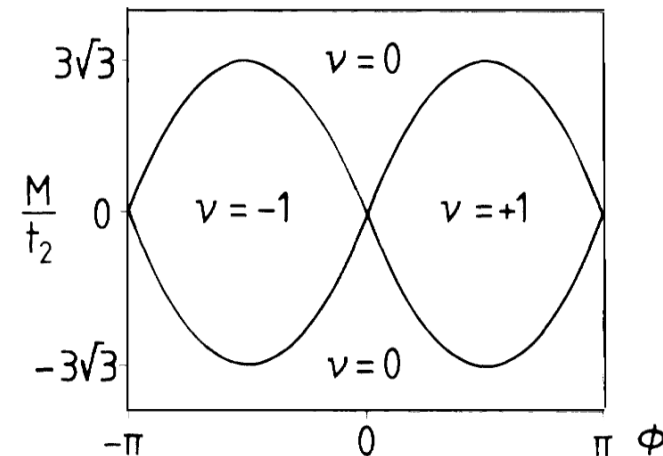


FIG. 2. Phase diagram of the spinless electron model with $|t_2/t_1| < \frac{1}{3}$. Zero-field quantum Hall effect phases ($\nu = \pm 1$, where $\sigma^{xy} = ve^2/h$) occur if $|M/t_2| < 3\sqrt{3}|\sin\phi|$. This figure assumes that t_2 is positive; if it is negative, ν changes sign. At the phase boundaries separating the anomalous and normal ($\nu=0$) semiconductor phases, the low-energy excitations of the model simulate undoubled massless chiral relativistic fermions.

Fractional Chern insulator

Physics

ABOUT BROWSE PRESS COLLECTIONS CELEBRATING 10 YEARS

Viewpoint: Fractional quantum Hall effect without Landau levels

June 6, 2011 • Physics 4, 46

E. Tang, J-W. Mei, and X-G. Wen, **Phys. Rev. Lett.** **106**, 236802 (2011)

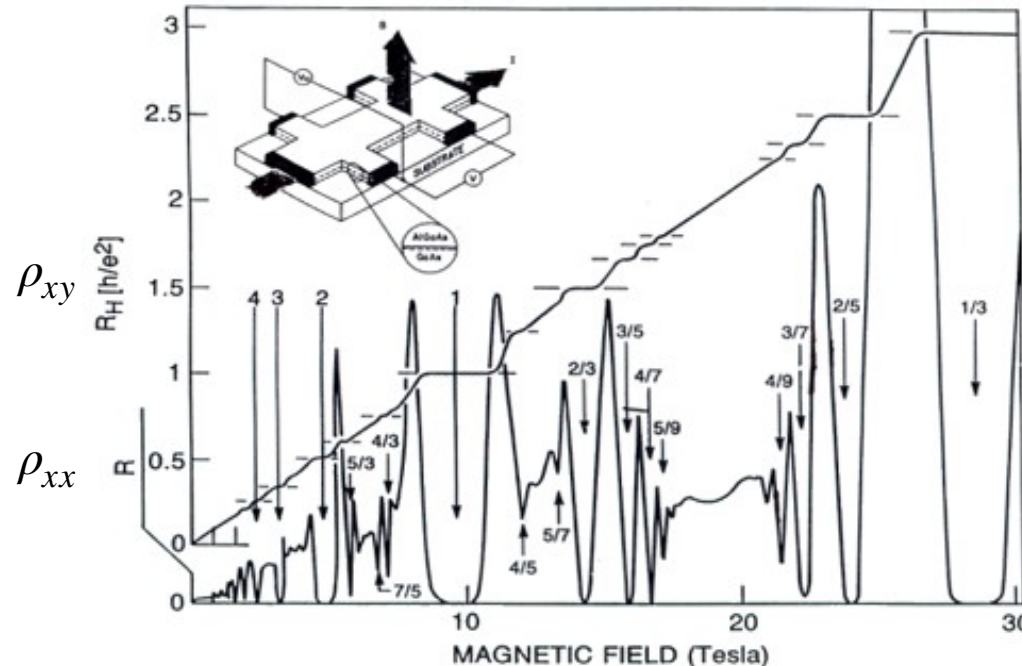
T. Neupert, L. Santos, C. Chamon, and C. Mudry, **Phys. Rev. Lett.** **106**, 236804 (2011)

K. Sun, Z. Gu, H. Katsura, and S. Das Sarma, **Phys. Rev. Lett.** **106**, 236803 (2011)

- researchers develop lattice models that could exhibit a fractional quantum Hall effect in the absence of an external magnetic field.
- non-trivial topological index + nearly flat bands = Landau level

Evidence of FQHE

- quantized Hall conductivity (fractional)



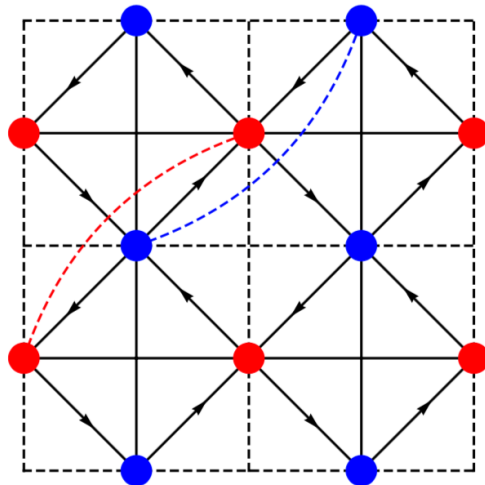
$$\rho_{xy} = \frac{1}{\nu} h/e^2$$

$$\sigma_{xy} = \nu e^2/h$$

$$\nu = \frac{1}{3}, \frac{2}{5}, \frac{3}{7}, \dots$$

- topological degeneracy of the ground states
- finite gap between ground state manifold and higher excited states
- fractional Chern number
- flow of the ground states into each other upon flux insertion

Topological flatband

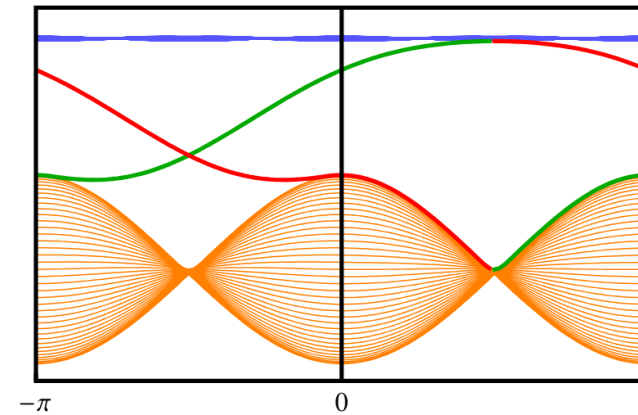
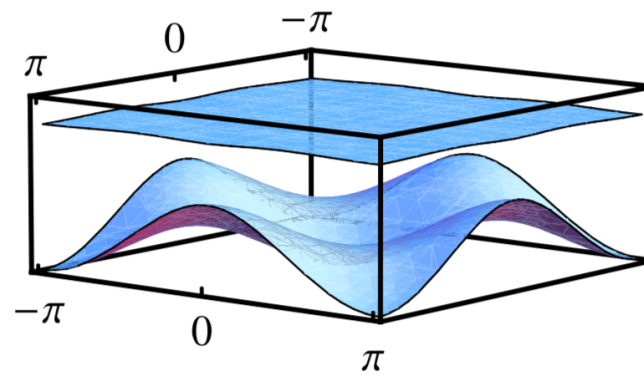


$$H = -t \sum_{\langle i,j \rangle} e^{i\phi_{ij}} (c_i^\dagger c_j + \text{H.c.}) - \sum_{\langle\langle i,j \rangle\rangle} t'_{ij} (c_i^\dagger c_j + \text{H.c.}) - t'' \sum_{\langle\langle\langle i,j \rangle\rangle\rangle} (c_i^\dagger c_j + \text{H.c.}),$$

$$t = 1, \quad t'_1 = -t'_2 = 1/(2 + \sqrt{2}), \quad t'' = 1/(2 + 2\sqrt{2})$$

$H = -\sum_{\vec{k}} \psi_{\vec{k}}^\dagger \mathcal{H} \psi_{\vec{k}}$, where $\psi_{\vec{k}} = (a_{\vec{k}}, b_{\vec{k}})$ is a two component spinor and \mathcal{H} is a 2×2 matrix

$$\begin{aligned} \mathcal{H} = & [(t'_1 + t'_2)(\cos k_x + \cos k_y) + 4t'' \cos k_x \cos k_y] I + 4t \cos \phi \left(\cos \frac{k_x}{2} \cos \frac{k_y}{2} \right) \sigma_x + 4t \sin \phi \left(\sin \frac{k_x}{2} \sin \frac{k_y}{2} \right) \sigma_y \\ & + (t'_1 - t'_2)(\cos k_x - \cos k_y) \sigma_z. \end{aligned}$$



+ fractional filling + interactions

$$H = -H_0 + U \sum_{\langle i,j \rangle} n_i n_j + V \sum_{\langle\langle i,j \rangle\rangle} n_i n_j$$

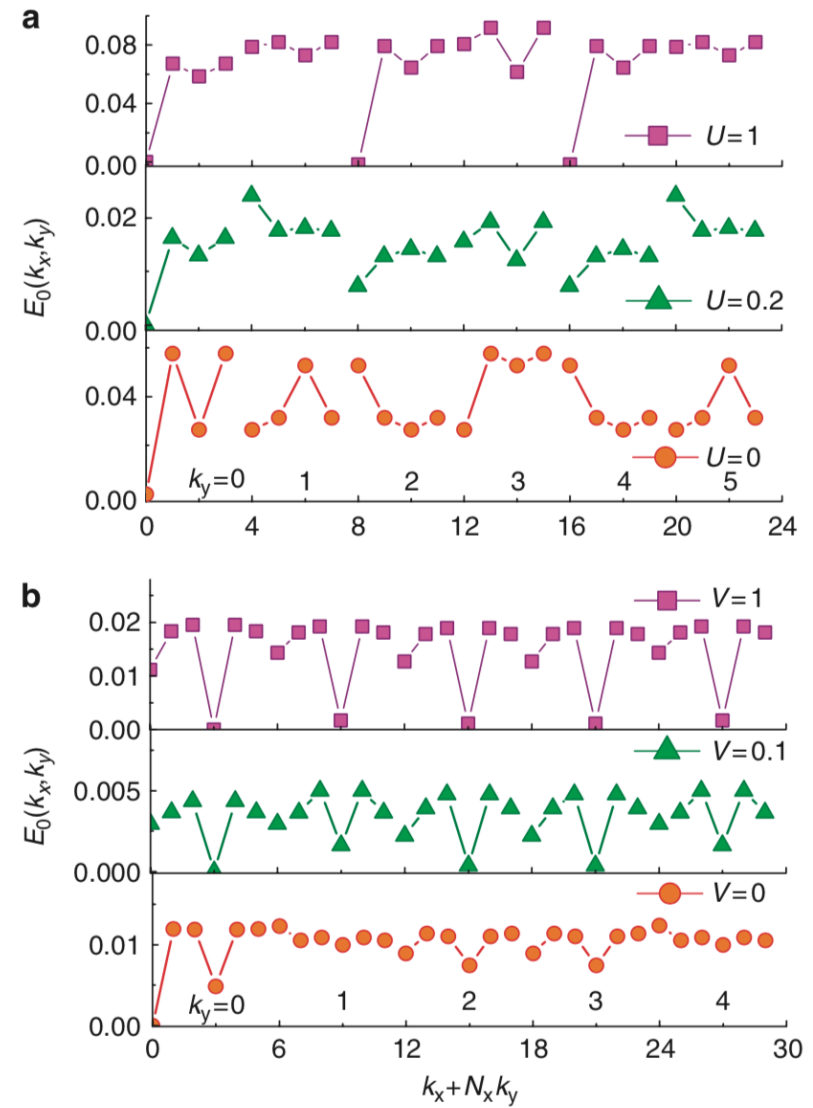
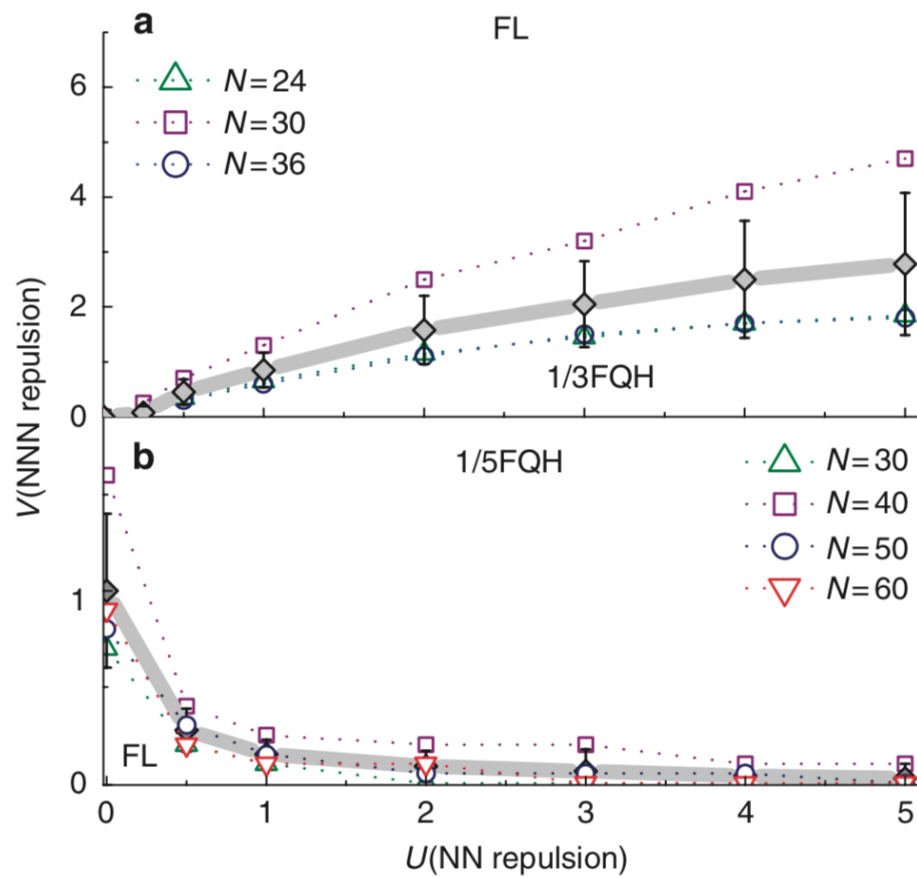


Figure 2 | Energy spectrum with interaction. (a) For 1/3 filling with $V=0$, $U=0$ to 1.0 (U increases from bottom panel up) and $N_s=2\times 4\times 6$ sites; (b) For 1/5 filling with $U=1$ and $V=0$ to $V=1$ and $N_s=2\times 6\times 5$. We have shifted the ground-state energy to zero for comparison. Nearly degenerate GSM and the large gap between GSM and excited states, observed in (a) at large U and (b) at large V indicate the formation of the fractional quantum Hall states.

Many-body Chern number

- the Chern number of a many-body state is an integral invariant in the boundary phase space

$$C = \frac{1}{2\pi} \int d\theta_x d\theta_y F(\theta_x, \theta_y)$$

where θ_x and θ_y are the boundary phases in x and y directions, and the Berry curvature is given by

$$F(\theta_x, \theta_y) = \text{Im} \left(\left\langle \frac{\partial \Psi}{\partial \theta_y} \frac{\partial \Psi}{\partial \theta_x} \right\rangle - \left\langle \frac{\partial \Psi}{\partial \theta_x} \frac{\partial \Psi}{\partial \theta_y} \right\rangle \right)$$

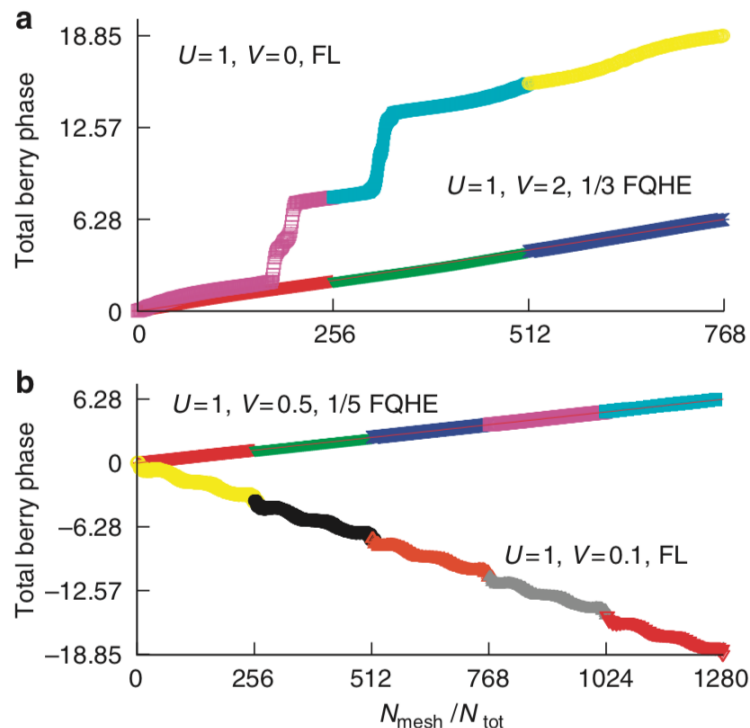
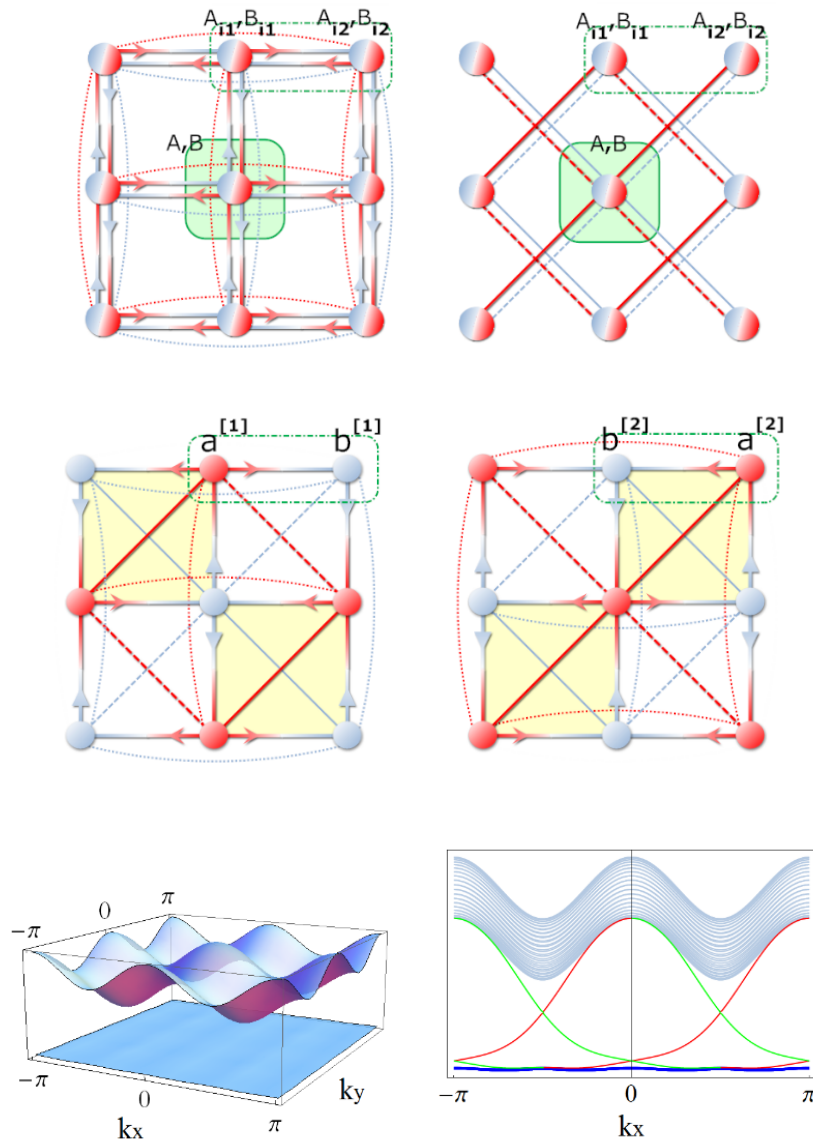


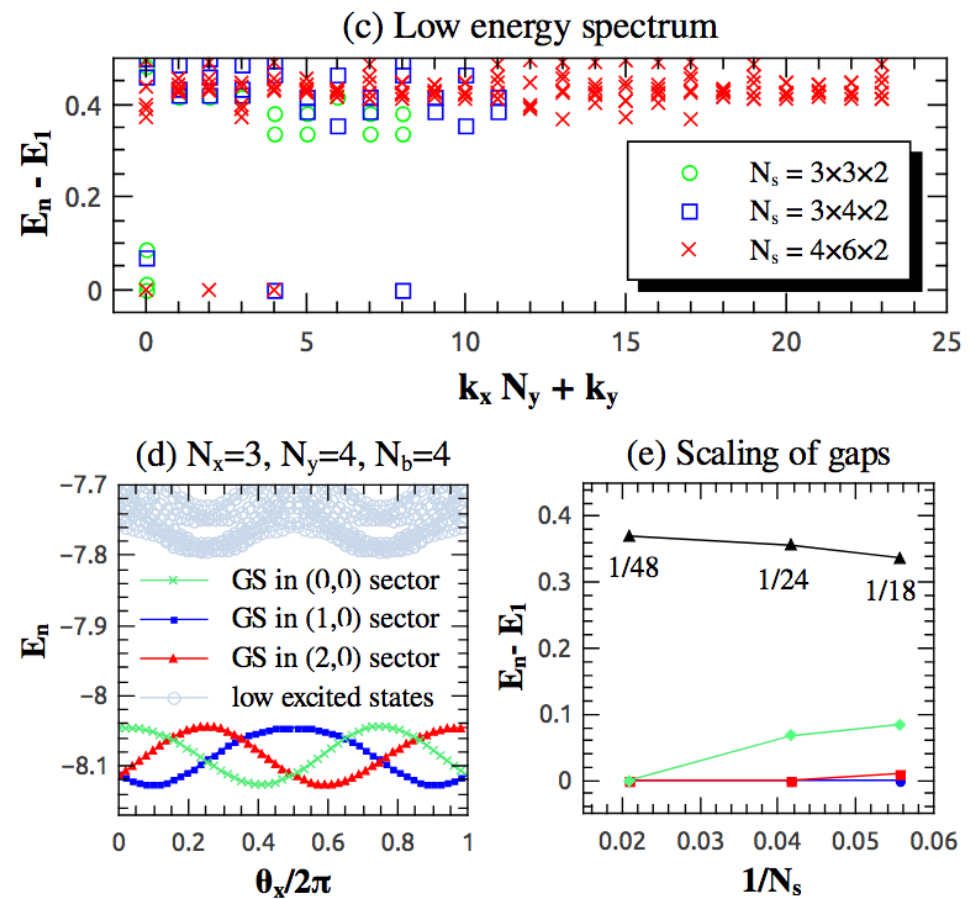
Figure 3 | Berry phase and topological quantization. The total Berry phase as a function of $N_{\text{mesh}}/N_{\text{tot}}$, which measures the ratio of the area in the boundary phase space for (a) 1/3 filling at $N_s = 30$; (b) 1/5 filling at $N_s = 40$. In fractional quantum Hall phase, a linear curve is observed whose slope is determined by filling factor, as expected. In the Fermi-liquid phase, we observed large fluctuation and non-universal behaviours, indicating the absence of the topological quantization.

fractional Chern number

Topological flatbands with higher Chern numbers



$$H^{[C=2]} = t_1 \sum_{\langle i,j \rangle} e^{i\phi_{ij}} A_i^\dagger B_j + \sum_{\langle\langle i,j \rangle\rangle} t'_{ij} (A_i^\dagger A_j + B_i^\dagger B_j) \\ + t_3 \sum_{\langle\langle\langle i,j \rangle\rangle\rangle} (A_i^\dagger A_j + B_i^\dagger B_j) + \text{H.c.},$$



S. Yang, Z.-C. Gu, K. Sun, and S. Das Sarma,
PRB 86, 241112(R) (2012)

- the 1/3 bosonic FQHE

Recent progress in experiments

nature

Explore content ▾ About the journal ▾ Publish with us ▾

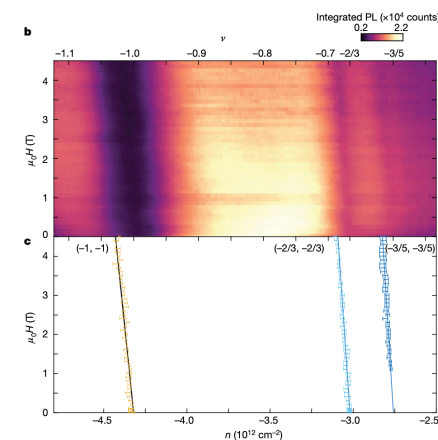
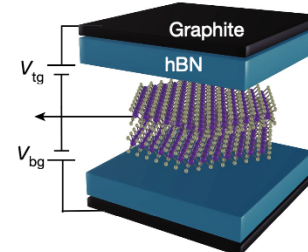
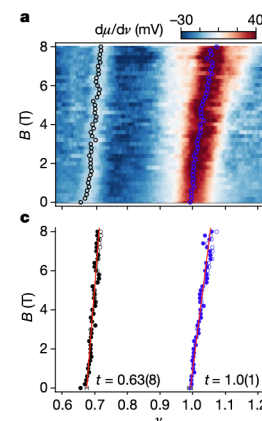
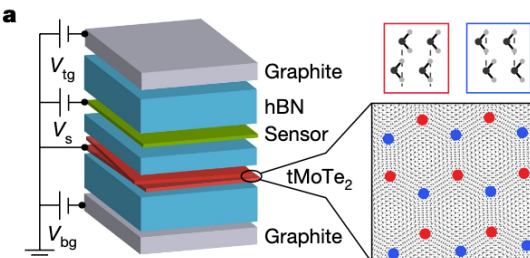
nature > articles > article

Article | Published: 14 June 2023

Signatures of fractional quantum anomalous Hall states in twisted MoTe₂

Jiaqi Cai, Eric Anderson, Chong Wang, Xiaowei Zhang, Xiaoyu Liu, William Holtzmann, Yinong Zhang, Fengren Fan, Takashi Taniguchi, Kenji Watanabe, Ying Ran, Ting Cao, Liang Fu, Di Xiao, Wang Yao & Xiaodong Xu

Nature 622, 63–68 (2023) | Cite this article



nature

Explore content ▾ About the journal ▾ Publish with us ▾

nature > articles > article

Article | Published: 26 July 2023

Thermodynamic evidence of fractional Chern insulator in moiré MoTe₂

Yihang Zeng, Zhengchao Xia, Kaifei Kang, Jiacheng Zhu, Patrick Knüppel, Chirag Vaswani, Kenji Watanabe, Takashi Taniguchi, Kin Fai Mak & Jie Shan

Nature 622, 69–73 (2023) | Cite this article

Science

Current Issue First release papers Archive About ▾

Submit ▾

HOME > SCIENCE > VOL. 384, NO. 6696 > LARGE QUANTUM ANOMALOUS HALL EFFECT IN SPIN-ORBIT PROXIMITIZED RHOMBOHEDRAL GRAPHENE

RESEARCH ARTICLE | 2D MATERIALS

Large quantum anomalous Hall effect in spin-orbit proximitized rhombohedral graphene

TONGHANG HAN, ZHENGGUANG LU, YUXUAN YAO, JIXIANG YANG, JUNSEOK SEO, CHIHO YOON, KENJI WATANABE, TAKASHI TANIGUCHI, LIANG FU, [...] AND LONG JU, +1 authors Authors Info & Affiliations

